

Title	Dynamical pattern formation in two-dimensional fluids and Landau pole bifurcation
Author(s)	Ogawa, Shun; Barré, Julien; Morita, Hidetoshi; Yamaguchi, Yoshiyuki Y.
Citation	Physical Review E (2014), 89(6)
Issue Date	2014-06-12
URL	http://hdl.handle.net/2433/188947
Right	©2014 American Physical Society
Type	Journal Article
Textversion	publisher

Dynamical pattern formation in two-dimensional fluids and Landau pole bifurcation

Shun Ogawa,^{1,*} Julien Barré,² Hidetoshi Morita,^{3,4} and Yoshiyuki Y. Yamaguchi¹

¹*Department of Applied Mathematics and Physics, Graduate School of Informatics, Kyoto University, 606-8501 Kyoto, Japan*

²*Laboratoire J. A. Dieudonné, Université de Nice Sophia-Antipolis, UMR CNRS 7351, Parc Valrose, F-06108 Nice Cedex 02, France*

³*Department of Mathematics, Kyoto University, 606-8502 Kyoto, Japan*

⁴*CREST, JST, 606-8502 Kyoto, Japan*

(Received 29 January 2014; published 12 June 2014)

A phenomenological theory is proposed to analyze the asymptotic dynamics of perturbed inviscid Kolmogorov shear flows in two dimensions. The phase diagram provided by the theory is in qualitative agreement with numerical observations, which include three phases depending on the aspect ratio of the domain and the size of the perturbation: a steady shear flow, a stationary dipole, and four traveling vortices. The theory is based on a precise study of the inviscid damping of the linearized equation and on an analysis of nonlinear effects. In particular, we show that the dominant Landau pole controlling the inviscid damping undergoes a bifurcation, which has important consequences on the asymptotic fate of the perturbation.

DOI: [10.1103/PhysRevE.89.063007](https://doi.org/10.1103/PhysRevE.89.063007)

PACS number(s): 47.54.-r, 47.15.ki, 05.45.-a

I. INTRODUCTION

Patterns in effective two-dimensional (2D) fluids flows are found in nature in various contexts [1,2]: atmospheric [3,4] and oceanic flows [5] are examples. To understand such large-scale patterns theoretically, the 2D Euler equation describing perfect fluids flows is a simplified starting point. In this context, the study of nonlinear structures, such as Kelvin's cat's eyes, over a shear flow has a long history [6–8], which includes more recent mathematical developments [9,10].

Statistical physics has often been invoked to explain the formation of large vortices since Onsager [11,12]. The Miller-Robert-Sommeria (MRS) theory [13–16], which constructs the microcanonical measure for 2D Euler flows by taking all the invariants into account, is a particularly successful achievement. A difficulty in applying this theory in practice is the fact that the 2D Euler equation has infinitely many invariants. More importantly, the theory assumes the vorticity field on the large scales to be stationary, and therefore it cannot describe nonstationary asymptotic behaviors. For these cases, the statistical physics approach should be supplemented by a dynamical understanding of pattern formations.

In this paper, we consider a shear base flow to which a perturbation is added, and we propose a phenomenological approach to the pattern formations by analyzing the Landau pole of the linearized equation with its bifurcation, and by taking into account nonlinear effects.

Detailed numerical simulations of this situation are presented in Ref. [17]: starting from a Kolmogorov flow on the doubly periodic domain $\mathbb{T}^2 = [0, 2\pi) \times [0, 2\pi\Gamma)$, a perturbation of size ϵ is added; depending on the parameters (ϵ, Γ) , the perturbation may fully damp, evolve into a stationary dipole, or create four long-lived traveling vortices. The regions on the (ϵ, Γ) plane where the dipole or traveling vortices appear are numerically investigated in Ref. [17], but a theoretical understanding is lacking. In this article, we aim at providing such a theoretical explanation by exploiting the analogy between the 2D Euler equation for the vorticity field and the

Vlasov equation for plasmas. Indeed, a similar phenomenon has been investigated in one-dimensional plasmas, described by the Vlasov equation. A naive linear theory predicts that perturbations added to stable stationary states damp exponentially [18]. It is well known, however, that if the perturbation is large enough, nonlinear effects come into play, prevent complete damping, and may create traveling clusters [19–22]; see also Ref. [23] for the simpler cases of a ferromagnetic and an antiferromagnetic Hamiltonian mean-field model. To be more precise, according to Refs. [19,23], such a phenomenon occurs when the following two criteria are satisfied:

(i) The Landau damping time scale is longer than a nonlinear time scale, called a “trapping time scale.”

(ii) If several clusters are formed, they should be so small that they do not overlap and that a nonlinear superposition approximation [24] may work.

Although these criteria are in view of nonlinear dynamics, they can be expressed using the dominant Landau pole computed from the linearized Euler equation. Our goal is to draw the phase diagram in the (ϵ, Γ) plane by using the above two criteria in the context of the Euler equation, that is, by combining the phenomenological nonlinear estimate and the linear Landau damping theory.

This article is organized as follows. In Sec. II, we qualitatively analyze criteria (i) and (ii), and we show that they are related to the imaginary and the real parts of the dominant Landau pole of the initial Kolmogorov flow. We therefore briefly review the linear theory for 2D incompressible and inviscid fluids, and we derive the dispersion relation in Sec. III; the computation of the Landau pole requires an analytic continuation procedure similar to the one used in Ref. [25]. Using these computations, we draw a phase diagram in the (ϵ, Γ) plane in Sec. IV, and we compare this phenomenological estimate with numerical simulations in Sec. V. Section VI is devoted to the summary and discussions.

II. THE CRITERIA TO OBSERVE A DIPOLE, OR TRAVELING VORTICES

We start from the 2D Euler equation in the domain \mathbb{T}^2 ,

$$\frac{\partial \omega}{\partial t} + \vec{v} \cdot \nabla \omega = 0, \quad (1)$$

*sogawa@amp.i.kyoto-u.ac.jp

where the vorticity field ω and the velocity field \vec{v} are related to a stream function ψ through

$$\omega = \nabla^2 \psi, \quad \vec{v} = \left(-\frac{\partial \psi}{\partial y}, \frac{\partial \psi}{\partial x} \right). \quad (2)$$

The periods for the x and y axes are set as 2π and $2\pi\Gamma$, respectively.

We consider the stationary Kolmogorov flow, called hereafter the “base flow,” whose stream function is $\psi_0 = -\Gamma \sin(y/\Gamma)$ and whose vorticity and velocity fields are, respectively,

$$\omega_0(y) = -U'(y), \quad \vec{v}_0 = (U(y), 0), \quad (3)$$

with $U(y) = \cos(y/\Gamma)$. We add a large-scale perturbation to the base flow, and we expand the stream function as

$$\psi(x, y, t) = \psi_0(y) + \psi_1(x, y, t), \quad (4)$$

with

$$\psi_1(x, y, t = 0) = \epsilon \cos x. \quad (5)$$

In our analytical computations, ϵ is assumed to be small; this restriction obviously does not hold for numerical simulations. Nevertheless, the theory will be qualitatively in good agreement with the simulations.

When the base flow is stable (this corresponds to an aspect ratio $\Gamma > 1$), the linear theory typically predicts that the perturbation damps and possibly oscillates at complex frequency $c = c_R + ic_I$ ($c_R, c_I \in \mathbb{R}$), where c is the root of the dispersion relation yielding the slowest damping, with frequency c_R . That is, c is the root closest to the real axis, or, in other words, with the smallest $|c_I|$. The idea is that while the perturbation damps, it will tend to create vortices, traveling in the x direction at velocity c_R , since the 2π periodicity in the x direction permits us to identify the frequency with the velocity. The vortices are, therefore, located on the lines $y = Y_*$ satisfying $U(Y_*) = c_R$; if nonlinear effects are strong enough, these vortices may persist for long times. We note that, in the present setting, if $c_R + ic_I$ is a root of the dispersion relation, then $-c_R + ic_I$ is also a root. One may, therefore, expect four traveling vortices if $c_R \neq 0$, while the formation of two stationary vortices (a dipole) should be favored if $c_R = 0$.

A. Criterion (i): Damping time scale longer than trapping time scale

The damping time scale τ_L is easily estimated as the inverse of the Landau damping rate $\tau_L \simeq 1/|c_I|$. Actually, in addition to the exponential Landau damping described by c_I , there is an algebraic damping coming from the branch points of the dispersion function (see Sec. III); however, the exponential Landau damping is expected to be dominant on the time scale considered in this paper.

Next, we estimate the “trapping time scale,” τ_T , which is the characteristic time scale concerning nonlinearities [19], as the period of a test point vortex trapped around the edge of a small vortex. The temporal evolution of the position of a test point vortex is governed by the velocity field

$$\dot{x} = -\frac{\partial \psi}{\partial y} = U(y) - \frac{\partial \psi_1}{\partial y}, \quad \dot{y} = \frac{\partial \psi}{\partial x} = \frac{\partial \psi_1}{\partial x}, \quad (6)$$

where the dot denotes d/dt . We approximate the perturbation $\psi_1(x, y, t)$ phenomenologically. We are interested in the macroscopic behavior corresponding to the $k = \pm 1$ modes, where k is the wave number with respect to x , and we assume that the damping perturbation has created small vortices whose velocity is c_R in the x direction; note that c_R can be 0. Since we have set the initial perturbation as Eq. (5), the first order $\psi_1(x, y, t)$ can be approximated by

$$\psi_1(x, y, t) \simeq \epsilon \hat{\psi}_1(y) \cos(x - c_R t), \quad U(y) \sim c_R, \quad (7)$$

where $\hat{\psi}_1(y)$ is of $O(\epsilon^0)$. Substituting Eq. (7) into Eq. (6), we have the approximate equations of motion

$$\dot{x} = U(y) - \epsilon \hat{\psi}'_1(y) \cos(x - c_R t), \quad (8)$$

$$\dot{y} = -\epsilon \hat{\psi}_1(y) \sin(x - c_R t),$$

where the prime represents d/dy . Thanks to the phenomenological approximation of ψ_1 (7), we can compute the motion of the test point vortex by perturbation techniques. Expanding x and y into series of ϵ as

$$x(t) = x_0(t) + \epsilon x_1(t) + O(\epsilon^2), \quad (9)$$

$$y(t) = y_0(t) + \epsilon y_1(t) + O(\epsilon^2),$$

we obtain the solutions $x_0(t)$ and $y_0(t)$ with initial conditions $x_0(0) = X$ and $y_0(0) = Y$:

$$x_0(t) = X + U(Y)t, \quad y_0(t) = Y. \quad (10)$$

Equations for the first order in ϵ are

$$\begin{aligned} \dot{x}_1(t) &= U'(Y)y_1(t) - \hat{\psi}'_1(Y) \cos(X + (U(Y) - c_R)t), \\ \dot{y}_1(t) &= -\hat{\psi}_1(Y) \sin(X + (U(Y) - c_R)t). \end{aligned} \quad (11)$$

From the frequency of y_1 in Eq. (11), we estimate the trapping time scale τ_T as

$$\tau_T \simeq \frac{1}{|U(Y_*) + g(\epsilon, \Gamma) - c_R|} \simeq \frac{1}{g(\epsilon, \Gamma)|U'(Y_*)|}, \quad (12)$$

where Y_* satisfies $U(Y_*) = c_R$, and $g(\epsilon, \Gamma) > 0$ represents the width of a vortex.

The unknown quantity, the width of a vortex $g(\epsilon, \Gamma)$, is determined self-consistently. The solution $y_1(t)$ is, from Eq. (11),

$$y_1(t) = \frac{\hat{\psi}_1(Y)}{U(Y) - c_R} (\cos(X + (U(Y) - c_R)t) - \cos X), \quad (13)$$

where the initial condition is $y_1(0) = 0$. The amplitude in the y direction, $\epsilon \hat{\psi}_1(Y)/[U(Y) - c_R]$, must be the same as the width $g(\epsilon, \Gamma)$ at the edge of the vortex, $Y = Y_* + g$. Thus, the self-consistent equation for g is

$$g = \frac{\epsilon}{U(Y_* + g) - c_R}, \quad (14)$$

where we have introduced another phenomenological approximation by replacing $\hat{\psi}_1(Y)$ with 1, since it is of $O(\epsilon^0)$ and we are looking for an order-of-magnitude estimate. The width g is, therefore, estimated as

$$g(\epsilon, \Gamma) \approx \sqrt{\frac{\epsilon}{|U'(Y_*)|}}. \quad (15)$$

For the Kolmogorov base flow, $U(y) = \cos(y/\Gamma)$, we have

$$|U'(Y_*)| = \frac{1}{\Gamma} \sqrt{1 - c_R^2}, \quad (16)$$

and the trapping time scale is

$$\tau_T = \sqrt{\frac{\Gamma}{\epsilon}} (1 - c_R^2)^{-1/4}. \quad (17)$$

Criterion (i) reads $\tau_T < \tau_L$, that is,

$$\frac{\Gamma c_1^2}{\sqrt{1 - c_R^2}} < \epsilon. \quad (18)$$

If $c_R = 0$, this condition simplifies into $\Gamma c_1^2 < \epsilon$.

B. Criterion (ii): Nonoverlapping vortices

We recall that the base flow is $U(y) = \cos(y/\Gamma)$, and the y positions of the vortices are estimated as $U(y) = \pm c_R$. The y positions and the width of vortices, g , give the nonoverlapping condition of vortices. We discuss the cases $c_R = 0$ and $c_R \neq 0$ separately.

If $c_R = 0$, one expects that vortices are formed at $y = \pi\Gamma/2$ and $3\pi\Gamma/2$. The estimate of the vortices width (15) shows that the vortices will never overlap for any reasonably small ϵ (say, for instance, $\epsilon < 0.5$). Hence criterion (ii) brings no restriction in this case.

If $c_R \neq 0$, in contrast, the vortices can be close one to another, and criterion (ii) leads to a restriction. We name the four vortices A , B , C , and D , whose y positions are, respectively, $\Gamma \arccos(|c_R|)$, $\pi\Gamma - \Gamma \arccos(|c_R|)$, $\pi\Gamma + \Gamma \arccos(|c_R|)$, and $2\pi\Gamma - \Gamma \arccos(|c_R|)$ in the interval $[0, 2\pi\Gamma)$, where we take the branch of solutions $0 \leq \arccos(|c_R|) \leq \pi/2$; see Fig. 1.

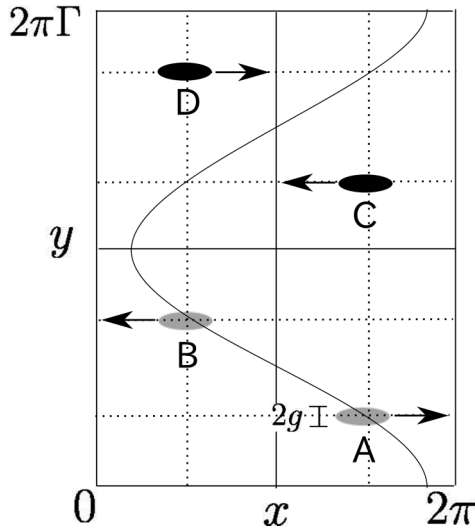


FIG. 1. Schematic picture of four traveling vortices, A , B , C , and D . The arrows indicate traveling directions. Vortices A and B have positive vorticity, while C and D have negative vorticity. The solid curve represents the velocity of the base flow $U(y)$, suitably rescaled. The two vertical dotted lines correspond to $\pm c_R$; their intersections with the velocity curve, $U(y) = \pm c_R$, yield the estimated y positions of the four vortices, which travel along the horizontal dotted lines.

We assume that each vortex has the same width g . Then the distance between two nearby vortices must be larger than $2g$ in order to avoid an overlap. Using $\pi/2 - \arccos(c_R) = \arcsin(c_R)$, this condition is expressed as

$$\begin{aligned} \Gamma \arcsin(c_R) &> g & (|c_R| < 1/\sqrt{2}), \\ \Gamma \arccos(c_R) &> g & (|c_R| > 1/\sqrt{2}). \end{aligned} \quad (19)$$

The first inequality comes from the distance in y between vortices A and B (identically C and D), and the second from the distance between B and C (identically A and D). The pair (B, C) moves toward the left while (A, D) moves toward the right according to the base flow $U(y)$. Moreover, the numerical observations [17] indicate that the difference in x among each pair stays around π . Thus the distance between B and C (A and D) is large enough to neglect the effect of overlapping; see Fig. 1. Hence we can omit the second inequality of Eq. (19), and criterion (ii) is finally expressed as

$$\epsilon < \Gamma \sqrt{1 - c_R^2} [\arcsin(c_R)]^2. \quad (20)$$

The two conditions (18) and (20) involve the parameters Γ and ϵ , as well as the dominant Landau poles $c = \pm c_R + ic_1$. In the following section, we turn to the computation of this Landau pole.

III. THE LINEAR THEORY AND THE DISPERSION RELATION

This section contains a classical computation for the linearized 2D Euler equation, as well as an analytic continuation in the spirit of Ref. [25], in order to make the paper self-contained.

A. The dispersion function $D(c)$

We linearize Eqs. (1) and (2) around the base flow (3). We add a small perturbation ψ_1 to $\psi_0(y)$, whose associated vorticity and velocity fields are denoted, respectively, as ω_1 and \vec{v}_1 . Substituting $\omega = \omega_0 + \omega_1$ and $\vec{v} = \vec{v}_0 + \vec{v}_1$ into the Euler equation (1) gives the linearized 2D Euler equation

$$\frac{\partial \omega_1}{\partial t} + \vec{v}_0 \cdot \nabla \omega_1 + \vec{v}_1 \cdot \nabla \omega_0 = 0. \quad (21)$$

Using the perturbation ψ_1 and Eq. (3), we rewrite the linearized Euler equation (21) as

$$\frac{\partial \omega_1}{\partial t} + U(y) \frac{\partial \omega_1}{\partial x} - U''(y) \frac{\partial \psi_1}{\partial x} = 0. \quad (22)$$

Our goal is now to derive the dispersion relation for the linearized Euler equation; we use a Fourier-Laplace transformation, and we follow the route of Ref. [26]. Thanks to the periodicity with respect to x , we expand ω_1 and ψ_1 into Fourier series as

$$\begin{aligned} \omega_1(x, y, t) &= \sum_{k \in \mathbb{Z}} \hat{\omega}_k(y, t) e^{ikx}, \\ \psi_1(x, y, t) &= \sum_{k \in \mathbb{Z}} \hat{\psi}_k(y, t) e^{ikx}. \end{aligned} \quad (23)$$

Substituting the Fourier expansions (23) into the linearized Euler equation (22), we obtain the equation for k th Fourier

mode as

$$\frac{\partial \hat{\omega}_k}{\partial t} + ikU(y)\hat{\omega}_k - ik\hat{\psi}_k U''(y) = 0, \quad \forall k \in \mathbb{Z}. \quad (24)$$

The Laplace transform of a function $\hat{g}(t)$ with respect to t is defined as

$$\tilde{g}(z) = \int_0^\infty \hat{g}(t)e^{-zt} dt, \quad \text{Re}z > 0, \quad (25)$$

where the condition $\text{Re}z > 0$ is introduced to ensure the convergence of the integral. Performing the Laplace transform of the linearized Euler equation (24), we obtain an algebraic equation for $\tilde{\omega}_k$ and $\tilde{\psi}_k$:

$$[U(y) - c]\tilde{\omega}_k - U''(y)\tilde{\psi}_k = \frac{\hat{\omega}_k(y,0)}{ik}, \quad (26)$$

where $z = -ikc$; note that $\text{Im}(kc) > 0$.

The Fourier transform of Eq. (2) with respect to x ,

$$\tilde{\omega}_k(y,c) = \left(\frac{\partial^2}{\partial y^2} - k^2 \right) \tilde{\psi}_k(y,c), \quad (27)$$

gives a closed equation for $\tilde{\psi}_k(y,c)$, which is the Rayleigh equation

$$\frac{\partial^2 \tilde{\psi}_k}{\partial y^2} - k^2 \tilde{\psi}_k - \frac{U''(y)}{U(y) - c} \tilde{\psi}_k = \frac{\hat{\omega}_k(y,0)}{ik[U(y) - c]}. \quad (28)$$

The stream function $\hat{\psi}_k(y,t)$ is computed through an inverse Laplace transform. Its asymptotic behavior is determined by the singularities of $\tilde{\psi}_k(y,c)$ with respect to the complex variable c . For simplicity, we introduce the functions q and f as

$$q(y) \equiv k^2 + \frac{U''(y)}{U(y) - c}, \quad f(y) \equiv \frac{\hat{\omega}_k(y,0)}{ik[U(y) - c]}. \quad (29)$$

These functions have no singularity for real y , since c is defined in the region $\text{Im}(kc) > 0$.

Fixing the complex variable c , we analyze the Rayleigh equation of the form

$$\frac{d^2 \phi}{dy^2} - q(y)\phi = f(y), \quad (30)$$

and the corresponding homogeneous Rayleigh equation

$$\frac{d^2 \phi}{dy^2} - q(y)\phi = 0. \quad (31)$$

Let ϕ_1 and ϕ_2 be independent solutions to the homogeneous equation (31) with boundary conditions

$$\begin{aligned} \phi_1(0) &= 1, & \phi_2(0) &= 0, \\ \phi_1'(0) &= 0, & \phi_2'(0) &= 1. \end{aligned} \quad (32)$$

The particular solution ϕ_p to the inhomogeneous equation (30) is then given by

$$\begin{aligned} \phi_p(y) &= -\phi_1(y) \int_0^y \phi_2(y') f(y') dy' \\ &\quad + \phi_2(y) \int_0^y \phi_1(y') f(y') dy'. \end{aligned} \quad (33)$$

Indeed, the double derivative of $\phi_p(y)$ is

$$\phi_p''(y) = q(y)\phi_p(y) + W(y)f(y), \quad (34)$$

where $W(y)$ is the Wronskian

$$W(y) = \phi_1(y)\phi_2'(y) - \phi_1'(y)\phi_2(y) \quad (35)$$

and is constant,

$$W(y) = W(0) = 1 \quad \text{for all } y. \quad (36)$$

Hence, the general solution ϕ_g to Eq. (28) is

$$\phi_g = \phi_p + a_1\phi_1 + a_2\phi_2, \quad (37)$$

where a_1 and a_2 are constants determined from the periodic boundary condition

$$\phi_g(2\pi\Gamma) = \phi_g(0), \quad \phi_g'(2\pi\Gamma) = \phi_g'(0). \quad (38)$$

From the boundary conditions (32) and $\phi_p(0) = \phi_p'(0) = 0$, Eqs. (37) and (38) lead to

$$\begin{pmatrix} \phi_1(2\pi\Gamma) - 1 & \phi_2(2\pi\Gamma) \\ \phi_1'(2\pi\Gamma) & \phi_2'(2\pi\Gamma) - 1 \end{pmatrix} \begin{pmatrix} a_1 \\ a_2 \end{pmatrix} = - \begin{pmatrix} \phi_p(2\pi\Gamma) \\ \phi_p'(2\pi\Gamma) \end{pmatrix}. \quad (39)$$

Remembering that $q(y)$ and hence ϕ_1 and ϕ_2 depend on c , we define the function $D(c)$ as

$$\begin{aligned} D(c) &= \det \begin{pmatrix} \phi_1(2\pi\Gamma) - 1 & \phi_2(2\pi\Gamma) \\ \phi_1'(2\pi\Gamma) & \phi_2'(2\pi\Gamma) - 1 \end{pmatrix} \\ &= 2 - \phi_1(2\pi\Gamma) - \phi_2'(2\pi\Gamma). \end{aligned} \quad (40)$$

To show the last equality in Eq. (40), we have used the fact that the Wronskian $W(y)$ is unity. The values of $\phi_1(2\pi\Gamma)$ and $\phi_2'(2\pi\Gamma)$ are computed by integrating the homogeneous Rayleigh equation (31) from 0 to $2\pi\Gamma$.

B. Analytic continuation of $D(c)$

The general solution (37) has singularities for c satisfying $D(c) = 0$, and these singularities yield nontrivial modes proportional to e^{-ikct} by the inverse Laplace transform. This justifies our terminology ‘‘dispersion relation’’ for $D(c) = 0$, and ‘‘dispersion function’’ for the function $D(c)$. Recall that the dispersion function $D(c)$ is *a priori* defined only in the region $\text{Im}(kc) > 0$ to ensure the convergence of the Laplace transform. To find roots giving stable modes, we analytically continue $D(c)$ for the whole complex c plane, in a similar manner to what has been performed for the Euler equation on the 2D disk [25,27,28].

Hereafter, we set $k = 1$ without loss of generality, and we take the particular form of the base flow: $U(y) = \cos(y/\Gamma)$. Corresponding to a given c , the functions $q(y)$ and $f(y)$ have singularities at which the equation $U(y) - c = 0$ is satisfied. Such singular points are, together with the integration paths of the homogeneous Rayleigh equation (31), schematically illustrated in Fig. 2 for both the cases $\text{Im}c > 0$ and $\text{Im}c < 0$. The integration paths are determined as follows.

For c on the upper half-plane, $D(c)$ is simply defined by integrating Eq. (31) along the real y axis, namely along the integration path:

$$L = \{y \in \mathbb{R} | y = y(s) = 2\pi\Gamma s, s \in [0,1]\}. \quad (41)$$

Continuously moving c to the lower half-plane allows us to define $D(c)$ for $\text{Im}c < 0$. If the path taking c from the upper to the lower half-plane crosses the singular interval $c \in [-1,1]$,

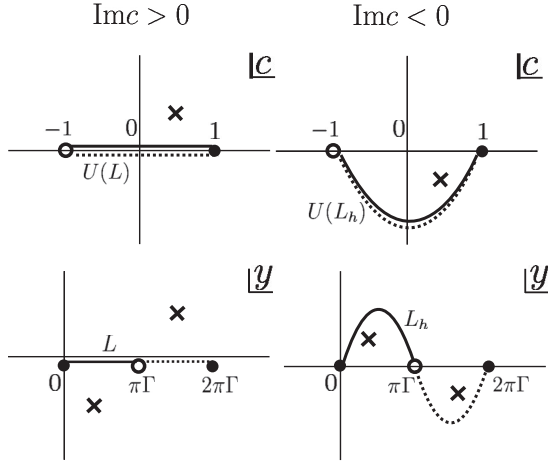


FIG. 2. Schematic picture of complex c and y planes for $k = 1$. The left two panels are for $\text{Im}c > 0$, and the right two panels are for $\text{Im}c < 0$. The integration path L on the y plane, consisting of the solid and the dotted lines, is mapped to the double covering of the interval $[-1, 1]$ on the c plane by the mapping $U : y \mapsto U(y)$. Corresponding to a given cross point on the c plane, there are two singular points (crosses) of $q(y)$ and $f(y)$ on the y plane in general. As the point on the c plane goes down, the singular points on the y plane pass the real axis and the integration path L must be deformed to L_h to avoid the singularities. The mapping of L_h , denoted by $U(L_h)$, determines the boundary of the continued domain of the dispersion function $D(c)$. See Fig. 3. A branch cut on the c plane is set as the boundary.

we have to avoid the singularity that would be created. For this purpose, we deform the integration path L to

$$L_h = \{y \in \mathbb{C} | y = y_h(s) = 2\pi\Gamma[s + ih(s)], s \in [0, 1]\}, \quad (42)$$

using a C^2 -class, real-valued, and 1-periodic function $h(s)$ satisfying $h(0) = h(1) = 0$; correspondingly, this amounts to deforming the singular line,

$$\sigma = \{c \in \mathbb{R} | c = U(y(s)), s \in [0, 1]\}, \quad (43)$$

which doubly covers the interval $[-1, 1]$, to the curve

$$\sigma_h = \{c \in \mathbb{C} | c = U(y_h(s)), s \in [0, 1]\}. \quad (44)$$

We choose the function $h(s)$ so that the deformed curve σ_h is below the c for which we want to define $D(c)$. This procedure is similar to the spectral deformation for the Vlasov-Poisson equation in Refs. [29,30].

If the path taking c from the upper to the lower plane crosses the real axis through either one of the half-lines $(-\infty, -1)$ or $(1, \infty)$, no singularity is crossed, and the analytic continuation does not require any deformation of the integral path; in the lower half-plane, $D(c)$ is multivalued unless a Riemann surface associated with the branch points $c = \pm 1$ is introduced.

We choose the particular deformation function $h(s)$ in Eq. (42) as

$$h(s) = a \sin 2\pi s, \quad a \geq 0. \quad (45)$$

The extended domains of $D(c)$ are shown in Fig. 3 for two different values of a . We use a large enough so that σ_h is below c ; the computational cost increases exponentially with increasing a .

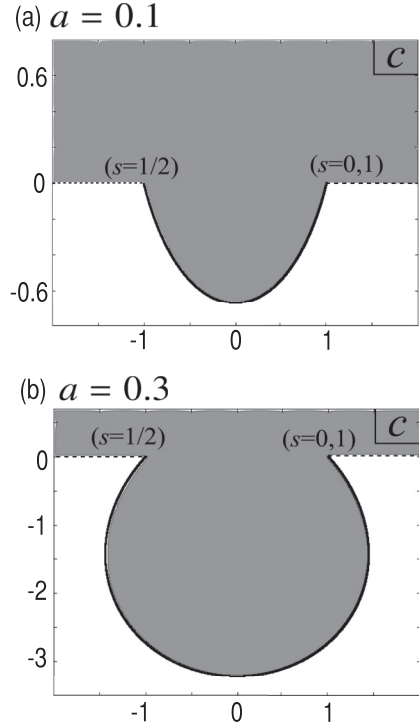


FIG. 3. Extension of the domain of $D(c)$. The gray regions represent the domains of $D(c)$ for (a) $a = 0.1$ and (b) $a = 0.3$. The curve in the c plane represents $U(y_h(s))$, where $y_h(s)$ is the deformed integration path for the homogeneous Rayleigh equation (31). With increasing a , the domain of $D(c)$ is extended to a larger area in the lower half c plane, but the computational cost also increases.

By introducing the following functions of s :

$$\varphi(s) = \phi(y_h(s)), \quad p(s) = q(y_h(s)), \quad (46)$$

the homogeneous Rayleigh equation (31) is rewritten as

$$\begin{aligned} \varphi''_R - \frac{h'h''}{1+h^2}\varphi'_R + \frac{h''}{1+h^2}\varphi'_I \\ - (2\pi\Gamma)^2[(1-h^2)p_R - 2h'p_I]\varphi_R \\ + (2\pi\Gamma)^2[2h'p_R + (1-h^2)p_I]\varphi_I = 0, \\ \varphi''_I - \frac{h''}{1+h^2}\varphi'_R - \frac{h'h''}{1+h^2}\varphi'_I \\ - (2\pi\Gamma)^2[2h'p_R + (1-h^2)p_I]\varphi_R \\ - (2\pi\Gamma)^2[(1-h^2)p_R - 2h'p_I]\varphi_I = 0, \end{aligned} \quad (47)$$

where the subscripts “R” and “I” represent the real and imaginary parts, respectively, and the prime denotes the derivative with respect to s . The continued solutions φ_1 and φ_2 are computed by solving Eq. (47) with the boundary conditions

$$\begin{aligned} \varphi_{1,R}(0) &= 1, & \varphi_{2,R}(0) &= 0, \\ \varphi_{1,I}(0) &= 0, & \varphi_{2,I}(0) &= 0, \\ \varphi'_{1,R}(0) &= 0, & \varphi'_{2,R}(0) &= 2\pi\Gamma, \\ \varphi'_{1,I}(0) &= 0, & \varphi'_{2,I}(0) &= 2\pi\Gamma h'(0), \end{aligned} \quad (48)$$

respectively. Solving Eq. (47), we obtain $\varphi_1(1)$ and $\varphi_2'(1)$, and the dispersion function is expressed as

$$D(c) = 2 - \varphi_1(1) - \frac{\varphi_2'(1)}{2\pi\Gamma(1 + ih'(1))}, \quad (49)$$

whose real and imaginary parts are, respectively,

$$\begin{aligned} D_R(c) &= 2 - \varphi_{1,R}(1) - \frac{\varphi_{2,R}(1) + h'(1)\varphi_{2,I}(1)}{2\pi\Gamma(1 + h'(1)^2)}, \\ D_I(c) &= -\varphi_{1,I}(1) + \frac{h'(1)\varphi_{2,R}(1) - \varphi_{2,I}(1)}{2\pi\Gamma(1 + h'(1)^2)}. \end{aligned} \quad (50)$$

C. The main Landau pole and its bifurcation

Using the analytical continuation of $D(c)$ into the lower half-plane, we numerically compute Landau poles, i.e., the roots of the equation $D(c) = 0$ with $\text{Im}c < 0$. We are interested in the traveling vortices, whose velocity is c_R , in resonance to the base flow, whose velocity $U(y)$ is in the range $[-1, 1]$. It is therefore natural to choose the analytical continuation of $D(c)$ defined by deforming the integral path as in Eq. (45).

We look for the dominant Landau pole, i.e., the root of $D(c)$ with the largest imaginary part; in a stable situation, it corresponds to the slowest damping. The variation of this pole as a function of the aspect ratio Γ is shown in Fig. 4. For $\Gamma < 1$, the flow is unstable. With increasing Γ above 1, the flow becomes stable, with the main Landau pole on the imaginary axis. With further increasing Γ , the dominant Landau pole

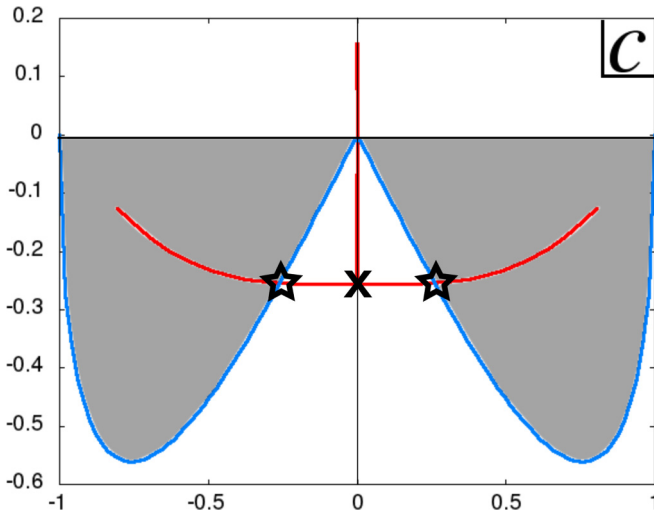


FIG. 4. (Color online) The dominant roots of the dispersion function (red line) and a favorable region for the existence of traveling vortices (gray region) on the complex c plane. When $\Gamma < 1$, one dominant root is obtained on the upper half-plane, where the base flow is unstable, and the root is at the origin for $\Gamma = 1$. With increasing Γ , the main root goes down to the lower half-plane along the imaginary c axis, accompanied by another root going up the axis. When $\Gamma = \Gamma_c \simeq 1.06$, these two roots collide at $c = -0.28i$ and they bifurcate to the right and left directions. The gray region is given by the inequality, $c_1^2 < (1 - c_R^2)[\arcsin(c_R)]^2$ coming from Eq. (51), and $c_1 < 0$ required by the stability of the flow. For later convenience, we marked the bifurcation point corresponding to $\Gamma = \Gamma_c$ by a cross, and the point at which the main pole enters the gray region by stars.

undergoes a bifurcation at an aspect ratio $\Gamma_c \simeq 1.06$ and acquires a nonzero real part. We will see that this bifurcation is crucial to understanding the appearance of a stationary dipole or of the four traveling vortices.

IV. THE PHASE DIAGRAM

Using the theoretical analyses given above, we construct the phase diagram on the (ϵ, Γ) plane, which consists of zonal,

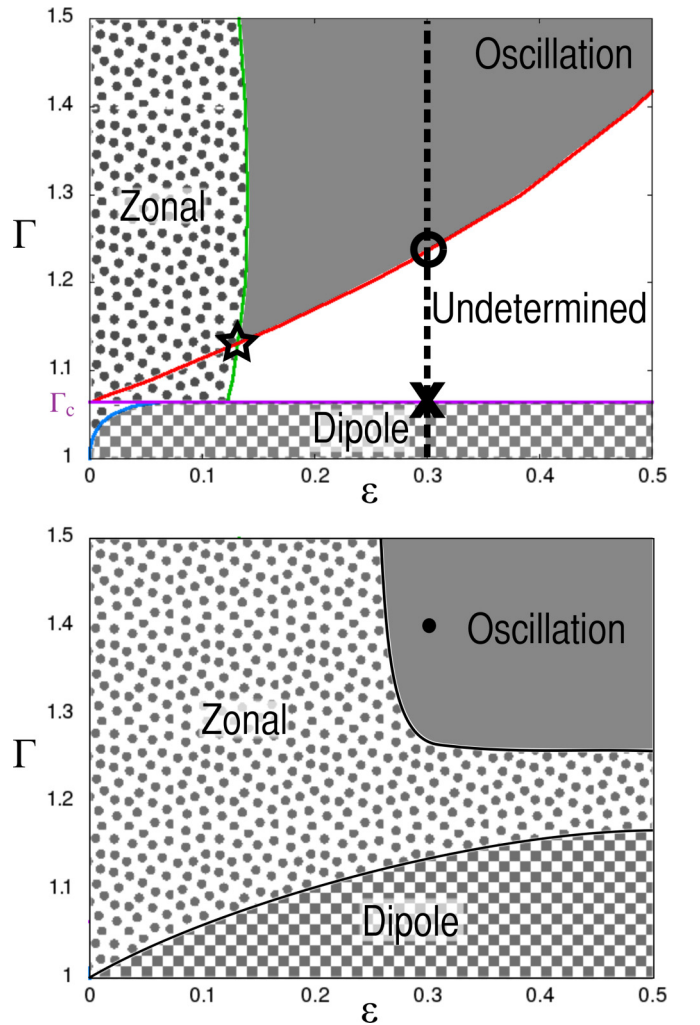


FIG. 5. (Color online) Phase diagram on the (ϵ, Γ) plane. The gray, polka-dotted, and checkered regions correspond to the oscillatory, zonal, and dipole phases, respectively. The upper panel is determined by the present theory and the lower is a schematic picture of the phase diagram obtained with the numerical simulations by Morita [17]. In the upper panel, the gray region is obtained from the inequality (51). The left green boundary of the gray region is given by $\epsilon = \Gamma c_1^2 / \sqrt{1 - c_R^2}$ [see Eq. (18)], and the lower red by $\epsilon = \Gamma \sqrt{1 - c_R^2} (\arcsin c_R)^2$ [see Eq. (20)]. The left blue boundary of the checkered region is given by $\epsilon = \Gamma c_1^2$, and the upper purple by $\Gamma = \Gamma_c$ [see Eq. (52)], whose value is determined at the bifurcation point marked by the cross in Fig. 4. The star point corresponds to the star point of Fig. 4. The broken line represents $\epsilon = 0.3$, upon which the theoretical and numerical frequencies are compared in Fig. 7. The points marked by the cross and the circle correspond to those in Fig. 7.

dipole, and oscillation phases [17]. The last oscillation phase corresponds to the four traveling vortices.

To obtain the region on the (ϵ, Γ) plane where the appearance of four traveling vortices is expected, we combine criteria (i) and (ii), which are Eqs. (18) and (20), respectively, with the result on the dominant Landau pole. Satisfying both criteria then reads

$$\frac{\Gamma c_1^2}{\sqrt{1 - c_R^2}} < \epsilon < \Gamma \sqrt{1 - c_R^2 [\arcsin(c_R)]^2}. \quad (51)$$

The right inequality requires a Landau pole with nonzero c_R , which implies $\Gamma > \Gamma_c$. The region that satisfies Eq. (51) on the (ϵ, Γ) plane is reported in Fig. 5, which is qualitatively in good agreement with the numerically obtained oscillatory region [17]. We remark that $|c_R|$ increases when Γ is increased above Γ_c , staying smaller than $1/\sqrt{2}$ in the reported parameter region. This fact validates that we have omitted the lower condition in Eq. (19) to derive the second necessary condition.

We expect to find a stationary dipole when criterion (i) is satisfied and $c_R = 0$:

$$\Gamma c_1^2 < \epsilon \quad \text{and} \quad \Gamma < \Gamma_c. \quad (52)$$

The region satisfying these requirements is highlighted in Fig. 5. This theoretically estimated region is again in qualitative agreement with the region where a stationary dipole emerges in numerical simulations [17].

We expect a zonal flow when criterion (i) is not satisfied, that is,

$$\begin{aligned} \Gamma c_1^2 > \epsilon \quad \text{for} \quad \Gamma < \Gamma_c, \\ \frac{\Gamma c_1^2}{\sqrt{1 - c_R^2}} > \epsilon \quad \text{for} \quad \Gamma > \Gamma_c. \end{aligned} \quad (53)$$

Physically, this means that nonlinearity is not dominant and hence simple damping of the perturbation is expected. In Fig. 5, the zonal region appears for small ϵ .

In Fig. 5, there is a region where the theory makes no prediction; indeed, the vortices that would be created by the phenomenological mechanism considered above would be so close to one another that they would strongly interact; the final fate of the system is therefore beyond the scope of the present theory. We note that in this region, zonal flows, dipoles, and traveling vortices are observed numerically [17].

V. NUMERICAL TESTS

According to the phenomenological prediction of the preceding sections, the four traveling vortices run in the x direction along the four lines $y = y_*$ in $\mathbb{T}^2 = [0, 2\pi) \times [0, 2\pi\Gamma)$, where $y_* = \Gamma \arccos(\pm c_R)$, and their velocities are $U(y_*) = \pm c_R$. The period in the x direction is 2π ; hence the phenomenological theory predicts the frequency $f_{pt} = |c_R|/2\pi$ for the vorticity field ω .

We examine our phenomenological prediction by numerically observing the y positions of the four vortices and the oscillation frequency. The initial condition of the vorticity field is

$$\omega(x, y, 0) = \omega_0(x, y) - \epsilon \cos x \quad (54)$$

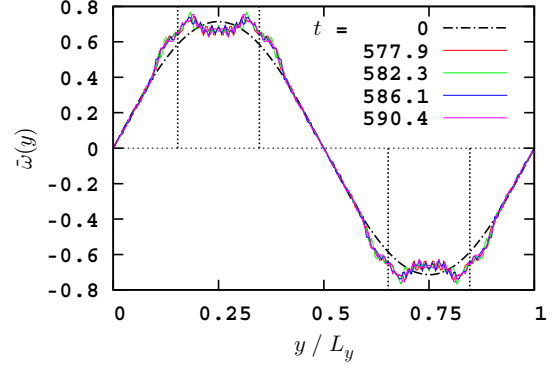


FIG. 6. (Color online) The averaged vorticity field $\bar{\omega}(y, t)$. Four bumps are observed, corresponding to four vortices in the long-time regime. The four vertical dotted lines indicate the theoretical predictions for the y positions of the vortices: $y/L_y = 0.25 \pm 0.097, 0.75 \pm 0.097$. $\Gamma = 1.4$ and $\epsilon = 0.3$.

fixing the small parameter $\epsilon = 0.3$. In numerical simulations, we add a hyperviscous term $(-1)^{h+1} \nu \nabla^{2h} \omega$ to the right-hand side of the 2D Euler equation, with $h = 4$ and $\nu = 2 \times 10^{-18}$, in order to stabilize the numerical scheme, that is, to remove numerical artifacts generated in the highest wave-number region due to finite-size effects. We use the pseudospectral method with the resolution 256×256 .

First, we observe the y positions by computing the averaged vorticity field $\bar{\omega}(y)$ defined by

$$\bar{\omega}(y, t) = \frac{1}{2\pi} \int_0^{2\pi} \omega(x, y, t) dx. \quad (55)$$

At the initial time $t = 0$, the averaged vorticity field is $\omega_0(y) = \sin(y/\Gamma)/\Gamma$, and it evolves in time. Asymptotically, we observe four bumps in $\bar{\omega}(y)$ as shown in Fig. 6 for $\Gamma = 1.4$

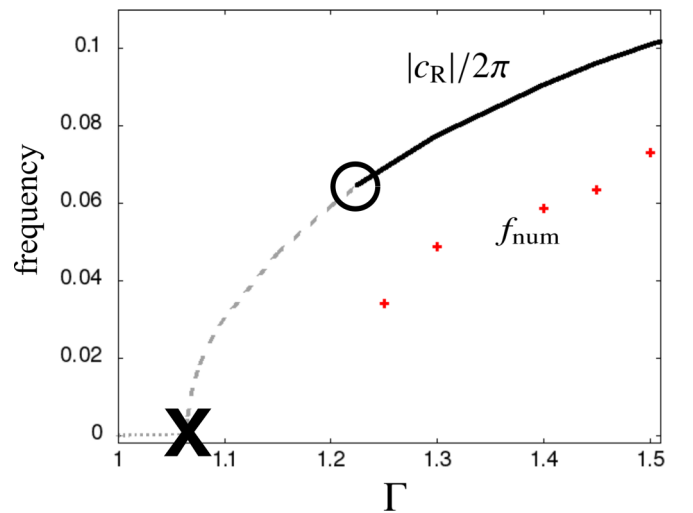


FIG. 7. (Color online) Γ dependence of the frequencies obtained from the theoretical prediction (bold curve) and the numerical simulations (red points). $\epsilon = 0.3$. Clear oscillation is not found by numerical simulations in the small Γ region, $\Gamma \lesssim 1.2$. The points marked by the cross and the circle correspond to those in Fig. 5.

and $\epsilon = 0.3$. The theoretical prediction is in good agreement with the numerically computed bump positions.

Next, we obtain the frequency by computing the power spectra of the (1,0) Fourier mode of $\omega(x, y, t)$ defined by

$$Z(t) = -\text{Re} \frac{1}{(2\pi)^2 \Gamma} \iint_{\mathbb{T}^2} \omega(x, y, t) e^{-ix} dx dy. \quad (56)$$

As shown in Fig. 7, the dependence on Γ of f_{num} is in qualitative agreement with the prediction, in the sense that the frequency increases as Γ increases. However, it is not in good agreement quantitatively. One possible explanation for the quantitative discrepancy in frequency is that $\epsilon = 0.3$ is too large to be considered a small perturbation to the base flow. The present theory is based on the linear analysis of the Euler equation. It gives good predictions qualitatively, but quantitatively nonlinear effects may kick in for rather large ϵ .

VI. SUMMARY AND DISCUSSIONS

Inspired by previous works on the Vlasov equation [19,22–24,31], we have considered (i) the balance between Landau damping and nonlinear effects, and (ii) the nonoverlapping criterion between nonlinear structures, in order to analyze the formation of a stationary dipole and traveling vortices in the 2D Euler equation starting from the perturbed stable Kolmogorov flow. The detailed linear analysis provides information on this nonlinear dynamical phenomenon. We emphasize that the bifurcation of the dominant Landau pole as the aspect ratio is varied plays a crucial role in the theory. Since this kind of bifurcation is probably not a special feature of the Kolmogorov flow, we expect that a similar analysis, predicting

the appearance, or not, of a dipole or traveling vortices, would be fruitful for other base flows.

We note that our prediction is in qualitative, though not quantitative, agreement with the numerical results of Ref. [17], not only for the shape of the phase diagram, but also for the vortex frequency. The quantitative discrepancy for the phase diagram is rather natural since we have performed phenomenological order-of-magnitude estimates, and we have not taken the prefactors into consideration. The reason for the quantitative disagreement in the frequency is probably that the size of the perturbation ϵ used in the numerical simulation is large enough to trigger nonlinear effects that we do not take into account, while such a large ϵ is necessary to realize the oscillating phase numerically.

We end this article by remarking that real fluid flows have viscosity, which brings higher-order derivative terms to the Euler equation [32]. These higher terms may dominate around the singularity on the y space, thus it is not obvious if our theory works in such viscous fluids, even for small viscosity. Analyzing viscous fluids in the spirit of Landau pole bifurcation is left for future work.

ACKNOWLEDGMENTS

The authors are grateful to F. Bouchet for fruitful discussions and comments on this study. S.O. acknowledges the hospitality of Université de Nice Sophia-Antipolis and the support of the JSPS Research Fellowships for Young Scientists (Grant No. 254728). This work was supported by the ANR-09-JCJC-009401 INTERLOP project. Y.Y.Y. acknowledges the support of a Grant-in-Aid for Scientific Research (C) 23560069.

-
- [1] F. Bouchet and A. Venaille, *Phys. Rep.* **515**, 227 (2012).
 [2] N. J. Balmforth, P. J. Morrison, and J. L. Thiffeault, [arXiv:1303.0065](https://arxiv.org/abs/1303.0065).
 [3] P. S. Marcus, *Nature (London)* **331**, 693 (1988).
 [4] B. Marston, *Physics* **4**, 20 (2011).
 [5] A. Venaille and F. Bouchet, *J. Phys. Ocean.* **41**, 1860 (2011).
 [6] W. Thomson, *Nature (London)* **23**, 45 (1880).
 [7] H. Lamb, *Hydrodynamics*, 6th ed. (Cambridge University Press, Cambridge, 1932).
 [8] J. T. Stuart, *J. Fluid Mech.* **29**, 417 (1967).
 [9] D. Holm, J. Marsden, and T. Ratiu, in *Nonlinear Systems of Partial Differential Equations in Applied Mathematics*, Lectures in Applied Mathematics Vol. 23 (American Mathematical Society, Providence, RI, 1986), Pt. 2, pp. 171–186.
 [10] Z. Lin and C. Zeng, *Arch. Rational Mech. Anal.* **200**, 1075 (2011).
 [11] L. Onsager, *Nuovo Cimento. Suppl.* **6**, 279 (1949).
 [12] G. L. Eyink and K. R. Sreenivasan, *Rev. Mod. Phys.* **78**, 87 (2006).
 [13] J. Miller, *Phys. Rev. Lett.* **65**, 2137 (1990).
 [14] J. Miller, P. B. Weichman, and M. C. Cross, *Phys. Rev. A* **45**, 2328 (1992).
 [15] R. Robert, *J. Stat. Phys.* **65**, 531 (1991).
 [16] R. Robert and J. Sommeria, *J. Fluids Mech.* **229**, 291 (1991).
 [17] H. Morita, [arXiv:1103.1140](https://arxiv.org/abs/1103.1140).
 [18] L. D. Landau, *J. Phys. U.S.S.R.* **10**, 25 (1946); *Collected Papers of L. D. Landau*, edited by D. T. Haar (Pergamon, Oxford, 1965).
 [19] T. M. O’Neil, *Phys. Fluids* **8**, 2255 (1965).
 [20] G. Manfredi, *Phys. Rev. Lett.* **79**, 2815 (1997).
 [21] M. Brunetti, F. Califano, and F. Pegoraro, *Phys. Rev. E* **62**, 4109 (2000).
 [22] C. Lancellotti and J. J. Dorning, *Phys. Rev. Lett.* **81**, 5137 (1998); *Phys. Rev. E* **68**, 026406 (2003); *Trans. Th. Stat. Phys.* **38**, 1 (2009).
 [23] J. Barré and Y. Y. Yamaguchi, *Phys. Rev. E* **79**, 036208 (2009).
 [24] M. Buchanan and J. J. Dorning, *Phys. Rev. Lett.* **70**, 3732 (1993); M. Buchanan and J. Dorning, *Phys. Rev. E* **52**, 3015 (1995).
 [25] R. L. Spencer and S. N. Rasband, *Phys. Plasmas* **4**, 53 (1997).
 [26] F. Bouchet and H. Morita, *Physica D* **239**, 948 (2010).
 [27] N. R. Corngold, *Phys. Plasmas* **2**, 620 (1995).
 [28] R. J. Briggs, J. D. Daugherty, and R. H. Levy, *Phys. Fluids* **13**, 421 (1970).
 [29] J. D. Crawford and P. D. Hislop, *Ann. Phys. (N.Y.)* **189**, 265 (1989).
 [30] P. D. Hislop and J. D. Crawford, *J. Math. Phys.* **30**, 2819 (1989).
 [31] J. P. Holloway and J. J. Dorning, *Phys. Rev. A* **44**, 3856 (1991).
 [32] A. V. Timofeev, *Sov. Phys. Usp.* **13**, 632 (1971).